Modeling of Projection Welding Processes Using Coupled Finite Element Analyses

A comprehensive thermal-electrical-mechanical analysis was performed to quantitatively simulate projection welding

BY X. SUN

ABSTRACT. Projection welding is a variation of resistance welding in which current flow is concentrated at the point of contact with a local geometric extension of one (or both) of the parts being welded. These extensions, or projections, are used to concentrate heat generation at the point of contact. The process typically uses lower currents, lower electrode forces and shorter welding times than does a similar application without the projection (Ref. 1). Because of the dynamic changes of the flow paths for heat and electrical current and the variation of the material properties with changing temperature, the process of projection welding, not unlike other resistance welding processes, is difficult to analyze. Earlier research on projection welding primarily relied on an all-experimental approach in which the heating process and nugget formation are qualitatively depicted using either consecutive metallurgical cross sections or high-speed movies. With the advances in computer technologies and finite element methods, a comprehensive analysis procedure has been developed to perform the incrementally coupled thermal-electrical-mechanical analysis to simulate the projection welding process in quantitative details. This analysis procedure is suitable for studying the electrical, thermal and mechanical aspects of the projection welding process such as the projection collapse mechanism, the nugget formation process and the effects of different welding parameters and base material properties. This new procedure can also be further developed to study many important parameters such as machine mechanical characteristics and their effect on nugget growth, contact area changes, dynamic resistance and electrode movement.

X. SUN is with Battelle Memorial Institute, Columbus, Ohio.

Introduction

Projection welding is an electrical resistance welding process in which welds are produced at localized points in workpieces held under pressure between suitable electrodes. As opposed to most other resistance welding processes, the precise location of the nugget (and weld) formation is predetermined and assured by the use of a bump (or projection) formed (or otherwise produced) between workpieces at their faying surfaces. It is a commonly used welding process in the appliance and automotive industries because of its high efficiency, consistency and low electrode wear. Like other resistance welding processes, many variables or parameters control the quality of a projection weld. Primarily, these parameters include projection design, electrode force, welding current, welding time and the type and thickness of the materials being welded.

KEY WORDS

Projection Welding
Finite Element Analysis
Welding Process Model
Projection Collapse
Projection Design
Nugget Growth

Many experimental research programs on projection welding were carried out between the 1940s and 1960s to study the influence of the aforementioned parameters on the projection collapse mechanism, weld size and weld performance. For example, Harris and Riley (Ref. 2) studied projection welding of low-carbon steel by cross sectioning the weld nuggets for consecutive weld times. The formation of the projection welds and the effects of welding variables such as welding currents, electrode force and welding time were qualitatively explained. Based on the knowledge accumulated from numerous experimental tryouts, some useful guidance was provided on the selection of welding equipment and process variables for welding low-carbon steels with embossed projections. Other researchers, such as Hess and Childs (Ref. 3), Hess, *et al.* (Ref. 4), Nippes, *et al.* (Ref. 5), Nippes and Gerken (Ref. 6) and Adams, *et al.* (Ref. 7), investigated the effects of different welding parameters and projection dimensions on weld formation and weld quality for both thin- and heavy-gauge materials such as AISI 1010 and AISI 1015. Cross-tension and lap-shear tests were conducted to relate the strength of the weld to the different welding parameters. It was also found that a spring-loaded electrode was necessary in welding thin-gauge material to provide rapid electrode follow up to prevent unwanted expulsion.

Starting in the mid 1960s, several researchers from the University of Texas at

Austin began to study the fundamentals of the projection welding process using high-speed photography (Refs. 8–10). Using high-speed movies of half welds, it was "possible to investigate weld collapse, effect of projection height, projection geometry, nugget formation, heat generation and flow, and weld quality in a manner not possible with any other technique (Ref. 8)."

More recently, Gould, *et al.* (Ref. 11), examined projection welding of coated sheet steels using metallurgical cross sections for consecutive time steps. It was concluded the stages of weld development for the coated steels varied markedly from those for uncoated steel. Using the same projection design, coated steels appeared to only experience solid-state bonding associated with projection collapse, as opposed to the formation of a fusion nugget in bare steel.

With the advances of computer technologies and finite element methods in the past two decades, it is now possible to model many different welding processes such as arc welding, friction welding and resistance spot welding (Refs. 12–20). These modeling techniques have been proven to be effective tools in understanding the physics of different welding processes, and in providing quantitative descriptions regarding the design and the performance characteristics of the resulting welds. However, probably because of the complexity involved in modeling of the projection welding process, no attempt has been reported in the open literature.

Several authors have used sequentially coupled finite element models to address different aspects of the resistance spot welding process such as nugget growth, electrode design and electrode wear. Among them are Nied (Ref. 12), Tsai, *et al.* (Ref. 13), Sheppard (Ref. 14), Murakawa (Ref. 15) and Dong, *et al.* (Ref. 16). Recently, Brown, *et al.* (Refs. 17 and 18), and Li, *et al.* (Ref. 19), presented the results of an incrementally coupled analysis of resistance spot welding of an aluminum alloy and steel, respectively, and the process dynamics of the resistance welding process was further explored. All of the above-mentioned incremental studies assume that the sheet geometry in the weld area does not change significantly during the welding process. Therefore, only changes in the contact areas obtained from the thermal-mechanical module are monitored and updated in the thermal-electrical analysis module (Refs. 17–19). However, this assumption is not valid in the case of projection welding in which the change of projection geometry during the initial heating cycles, *i.e.*, the projection collapse mechanism, is known to be the key factor influencing heat generation, nugget formation and weld quality. In order to account for the geometric changes in the projection area, a more complicated coupling procedure developed by Sun and Dong (Ref. 20) for resistance spot welding of aluminum must be employed. This coupling procedure updates both the contact area and the geometry of the projection area in the thermal-electrical analysis module according to the results obtained from the corresponding increment of the thermal-mechanical analysis module. By doing so, the projection collapse mechanism and nugget formation process are computed in an incrementally coupled manner.

The theoretical framework regarding the coupling effects of electrical-thermal-mechanical phenomena associated with spot welding presented in Ref. 20 is readily applied for the case of projection welding. The implementation of such an analysis procedure with a commercial code (*e.g.*, ABAQUS) and the incorpora-

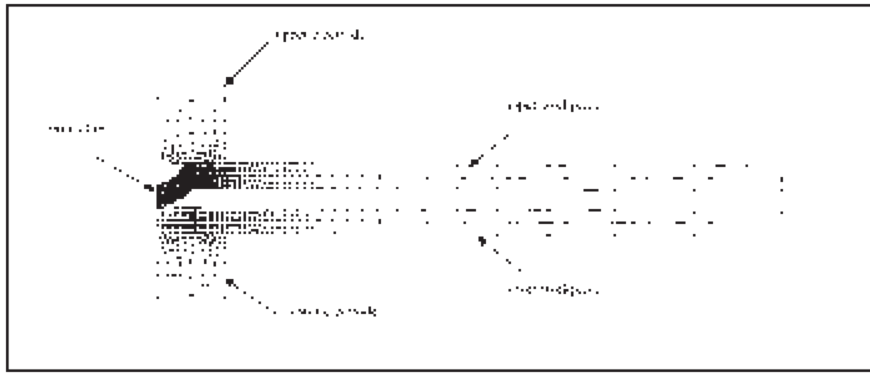

Fig. 1 —Typical finite element model.

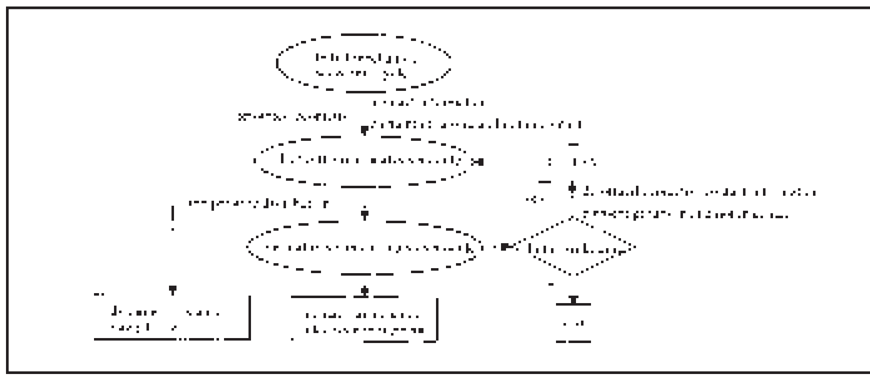

Fig. 2 —Flow chart of the coupled electrical-thermal-mechanical analysis.

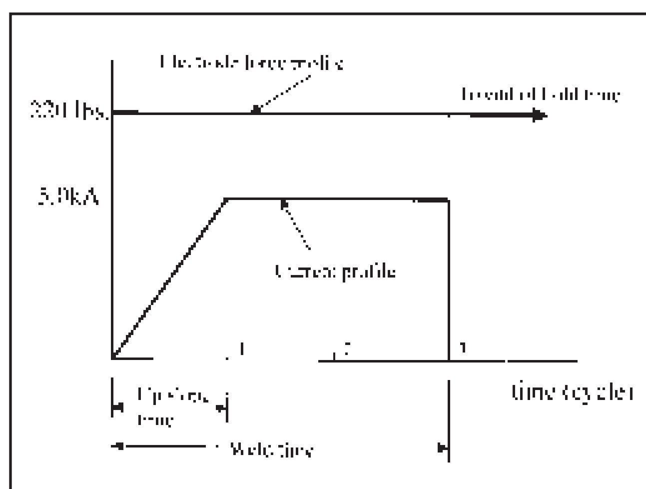

Fig. 3 — Illustration of welding parameters used in the case of SAE1010 steel sheet welding.

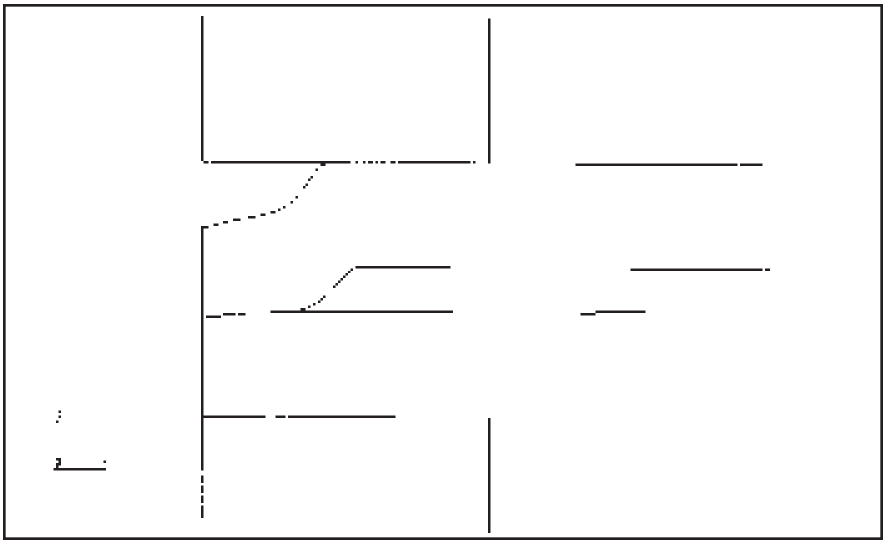

Fig. 4 — Cold collapse of projection after the squeeze cycle.

tion of appropriate boundary condition changes are discussed below. Some case studies regarding projection welding of 0.8-mm-gauge bare steel sheets are then presented. Projection collapse and nugget formation processes, and the effects of different updating frequency, sheet material property and welding parameters are finally discussed.

Finite Element Modeling Procedure

As pointed out by Sun and Dong (Ref. 20), there are currently no commercial FE codes available capable of solving the thermal-electrical-mechanical process in a fully coupled manner. An incrementally coupled finite element analysis procedure has been implemented in the current study. The analysis procedures are demonstrated here by using Fortran routines to link up different analysis modules of the commercial finite element code, *i.e.*, *ABAQUS* (Ref. 21).

A typical finite element mesh for half of the electrode-sheet assembly (as shown in Fig. 1) with axisymmetric condition being assumed can be employed without losing generality. The model consists of both three- and four-node linear elements, and a total of 841 elements are employed. The theory of large deformation is used to compute the excessive deformation of the projection. To facilitate the large plastic flow of material during projection collapse, three-node triangular elements are employed in the dimple area. Also, higher mesh density is used around sharp corners, as shown in Fig. 1.

The squeeze cycle is first modeled by a mechanical analysis. Uniformly distributed pressure calculated according to the specified electrode force is applied on the top of the upper electrode, and the bottom of the lower electrode is restrained from motion in the vertical direction. Contact surface interactions between the electrode-sheet interfaces and the faying interface are modeled with the concept of contact pair (Refs. 20 and 21). Contact pair is an option for modeling surface interactions in *ABAQUS* (Ref. 21). Instead of introducing a fictitious layer of solid interface elements at the contact surface, contact pair is a surface concept in which the master and slave surfaces of the contact are defined. The details of the contact pair formulation can be found in Ref. 20. Results generated from the squeezing cycle mechanical analysis, including deformed shape and coordinates, contact pressure, contact radius, element groups in and not in contact, etc., are first extracted, and then passed to the subsequent electrical-thermal analysis in which the welding current is applied.

In the electrical-thermal analysis, the deformed shape of the electrode-sheet assembly calculated from the previous mechanical analysis is used. Zero electrical potential is imposed on the bottom of the lower electrode tip, and distributed current density input calculated from the current input value is applied on the top of the upper electrode. All the free surfaces of the electrode and sheet assembly that are not in contact at this time increment are assumed to have free convection with the surrounding air, and the two electrodes are assumed to be water cooled with a forced-convection coeffi-

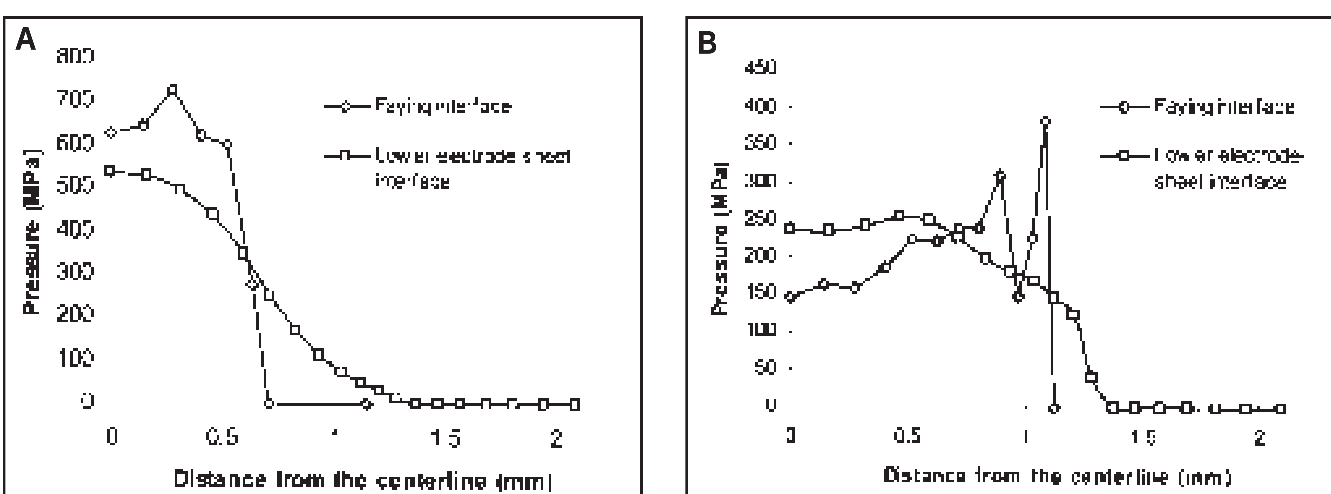

Fig. 5 — Pressure distribution along the faying interface and the lower electrode-sheet interface. A — Squeeze cycle; B — first cycle.

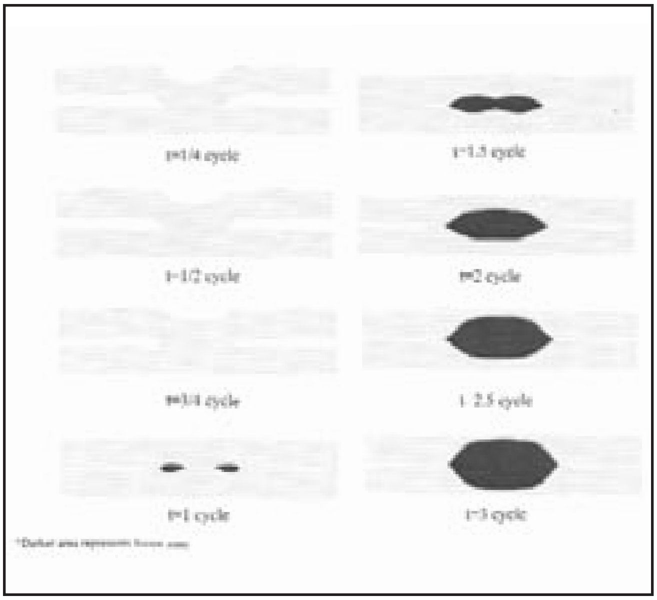

Fig. 6 — Predicted projection collapse and nugget formation process.

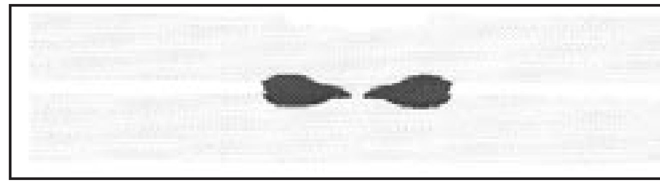

Fig. 7 — Molten zone shape and size at the end of the first cycle using updating frequency of ¼ cycle; onset of expulsion wrongly predicted.

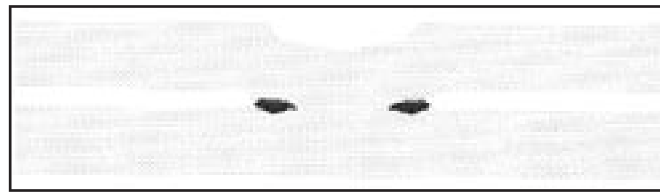

Fig. 8 — Predicted onset of expulsion at the end of the first half cycle using 8-kA welding current.

cient specified on their upper and lower free edges. Temperature-dependent material properties are used for both the electrode and the sheet during the entire modeling process. The surface electrical resistivity of the faying interface and the electrode sheet interface are computed by a user-interface subroutine following the formulation proposed by Li, *et al.,* in Ref. 19. The contact areas for the electrode-sheet interfaces and the faying interface are extracted from the previous mechanical analysis results to be used in the calculation of electrical contact resistivity. No pressure dependency is included in the current contact resistivity model, and the model has been used to successfully predict the nugget growth process for resistance spot welding of steel (Ref. 19).

The temperature distribution computed from the above electrical-thermal analysis for a certain time increment is then imposed as thermal loading conditions for the subsequent thermal-mechanical analysis module. This updating procedure repeats itself for a specific time increment, *i.e.*, updating frequency, until the entire welding cycle is totally completed. The flow chart of the analysis procedure is shown in Fig. 2. The entire analysis procedures were fully automated with the development of a suite of user-interface routines.

The modeling procedure described above is demonstrated next with some case studies simulating the projection welding processes of 0.8-mm-gauge bare steel sheets.

Results and Discussions

A typical finite element model is shown in Fig. 1 in which 0.8-mm-gauge bare steel sheets are welded using Harris and Riley (H&R) type projection (Refs. 1 and 2). The projection size and shape are determined according to Table 4 of Ref. 1 with its diameter and height being 2.29 mm and 0.635 mm, respectively, and its wall thickness being 90% of the sheet thickness. The electrodes used are flat-faced RWMA Class III type with a face radius of 2.3 mm.

Three- and four-node axisymmetric elements are used for the thermal-mechanical and electrical-thermal analysis. The mesh used in both analysis modules is shown in Fig. 1. Temperature-dependent material properties were used for both the workpieces and the copper electrodes (Refs. 22, 24 and 25). The cooling water temperature was set to be 22°C and convection effect was modeled by defining the temperature-dependent film coefficient using a user-interface subroutine. Because of the large deformation associated with the projection collapse process, a true stress and true strain curve must be used in the thermal-mechanical analysis. The following equations were used to derive the plastic material data from nominal stress and strain to true stress and strain (Ref. 21):

$$\sigma = \sigma_{nom}(1+\varepsilon_{nom}) \quad (1)$$

$$\varepsilon = 1n(1 + \varepsilon_{nom}) \quad (2)$$

It should be noted that the effect of strain rate on the strength of material was not taken into consideration in the current work. This is due to the lack of material data for such a high rate and high temperature event of projection welding. Should the rate data become available in the future, it can be easily incorporated in the simulation procedure by adding it to the input deck of the thermal-mechanical analysis module.

SAE1010 Steel Sheets

The first case analyzed is the projection welding of SAE1010 steel sheets using the projection shape shown in Fig. 1. The sheet material has a room-temperature nominal yield strength of 270 MPa, an ultimate strength of 310 MPa and an elongation of 32% (Refs. 3 and 6). The physical and mechanical properties for similar steel grades in elevated temperatures can be found in Refs. 22, 24 and 25. The absolute temperatures for the faying interface and the electrode-sheet interface are assumed to be 1500°C and 500°C for the calculation of surface contact resistivity (Ref. 19). The welding parameters used are welding current of 5 kA with linear up-slope control, constant electrode force of 220 lb and 3 welding cycles welding time, as recommended in Refs. 1 and 2 — Fig. 3.

It should be noted that, as some earlier studies have concluded, for welding thin-gauge materials, the welding machine's mechanical follow-up capacity has a strong influence on weld formation

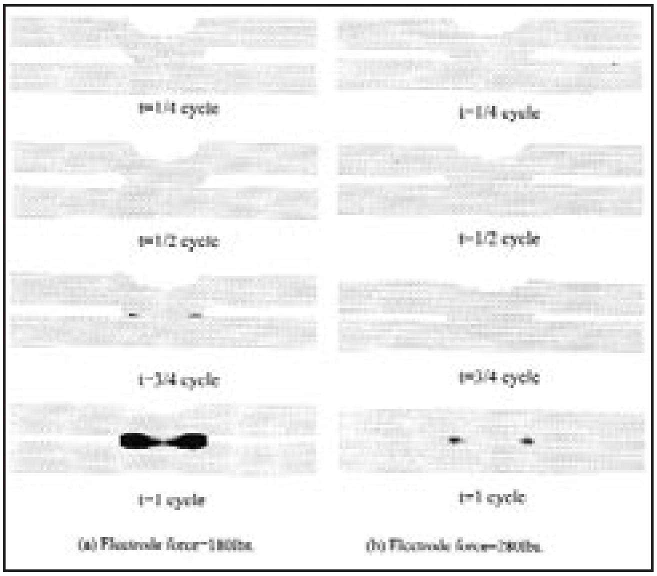

Fig. 9 — Effect of electrode force on projection collapse mechanism.

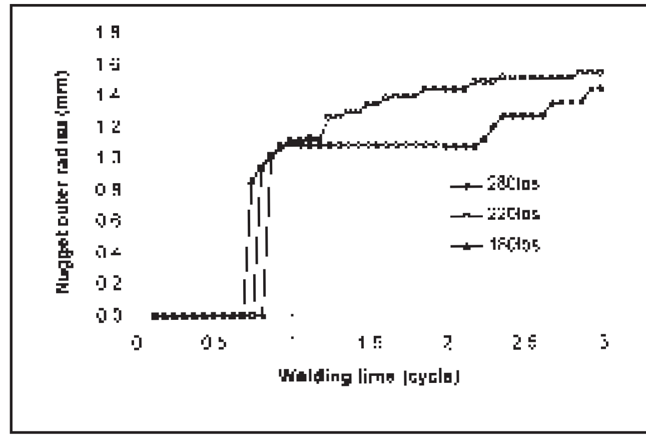

Fig. 10 — Nugget growth comparison for the three cases using different electrode forces.

and weld quality (Ref. 4), and sometimes a spring-loaded electrode is necessary to provide follow up rapid enough to prevent expulsion during welding (Ref. 5). In this study, it is assumed the electrode force during welding stays at a constant value of 220 lb. This is equivalent to assuming the welding machine has a perfect follow-up capability. It is certainly an idealized assumption. Nonetheless, at the current stage of research, the primary goal of this paper is to demonstrate the capability of the proposed coupled finite element modeling procedure. More realistic machine follow-up behavior can be added to this model by further specifying the electrode loading profile during welding for a specific welding machine or, more fundamentally, by directly incorporating the machine's mechanical characteristics, such as weld head mass, air cylinder pressure and friction coefficients, etc., into the nugget growth model.

Squeeze Cycle

At the end of the squeeze cycle, cold collapse of the projection occurs, and an area of intimate mechanical contact on the faying interface is established for the subsequent electrical current to pass through — Fig. 4. The amount of the vertical displacement of the upper electrode is 0.28 mm, or about 40% of the total projection height. Of this total amount, 0.07 mm is caused by the sheet-sheet indentation, and the rest is caused by the projection groove-face collapse. This indicates the particular projection shape and material combination chosen is not rigid enough to limit the cold collapse amount to be within 20% of the total projection height. This projection design and welding parameter combination is by no means optimized for this material. However, as will be shown later in the welding cycles, it does generate a satisfactory nugget.

The pressure distribution along the faying interface and lower electrode/sheet interface after the squeezing cycle is shown in Fig. 5A. The distribution characteristic along the faying interface very much resembles the classical elastic Hertzian contact problem with a cylindrical indentor. However, because of the loading-induced plasticity and limited projection wall thickness, a local pressure hump exists in the contact area as opposed to a smooth parabolic Hertzian solution (Ref. 23). The characteristics of the pressure distribution on the lower electrode/sheet interface is fundamentally different from the results obtained earlier for resistance spot welding with flat-tip electrodes (Refs. 13 and 20). Also, the contact diameters on all the interfaces are smaller than the electrode diameter.

Welding Cycle

The incrementally coupled electrical-thermal-mechanical simulation process commences once the welding current is fired. An updating frequency of 1⁄16 cycle was chosen for the entire three cycles of welding time. Consequently, the entire simulation result contains 48 thermal-electrical steps and 48 thermal-mechanical steps.

The pressure distribution along the faying interface and lower electrode/sheet interface after the first welding cycle is depicted in Fig. 5B. Comparing Figs. 5A and B, it is observed the contact radius on the lower electrode/sheet interface is almost unchanged from the squeeze cycle. However, at the end of the first cycle, the pressure distribution on this interface is much more uniform. The contact radius on the faying interface increases dramatically from the squeeze cycle to the first cycle. This indicates the progress of the projection collapse. The characteristics of the pressure distribution on the faying interface has also changed significantly from the squeeze cycle. At the end of the first cycle, the overall pressure distribution on the faying interface is similar to the elastic Hertzian problem with a flat indentor, with the exception of a low-pressure area close to the contact periphery where the highest nodal temperature is observed.

Figure 6 shows, at selective time frames, the heating and projection collapse patterns during the entire welding process. At the end of the first half cycle, the projection has collapsed more than 50% of its total height, and the current density concentrates at the outer ring location on the faying interface. At the end of the first cycle, the projection has totally collapsed, and a slight ring of indentation from the stamping process is still visible on the upper sheet surface — Fig. 6. Melting initiates in the form of a small ring on the faying interface as the result of high current density at the end of the first cycle. This heating pattern is consistent with the observations reported

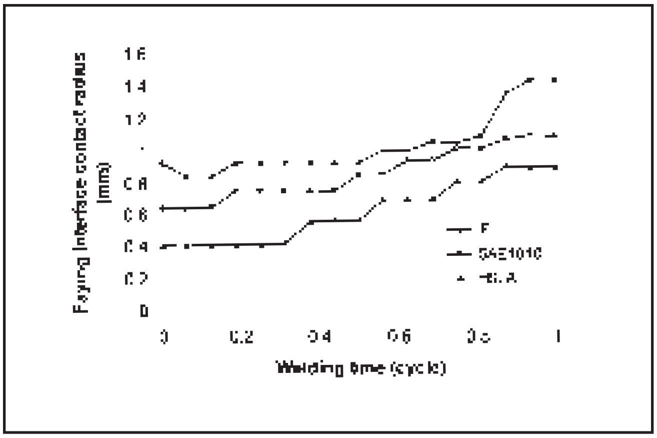

Fig. 11 — Comparison of contact radius for three different sheet materials.

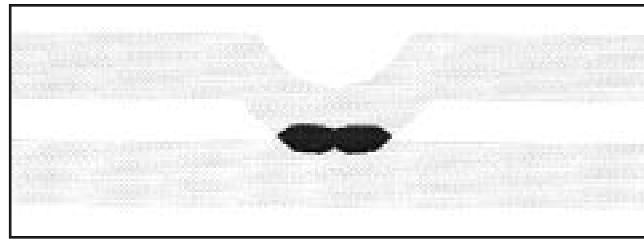

Fig. 12 — Predicted projection collapse and molten zone at the end of ½ cycle for HSLA steel.

in Ref. 9 from high-speed movies for this type of projection design. The result is also in line with most of the observations regarding the projection collapse process, which states “the collapse of the projection is practically complete before any fusion of the metal occurs” (Refs. 2, 3 and 11). At this time increment, the fine balance between the applied electrode force and the thermal expansion force of the molten zone is critical. If the machine’s follow-up capability is poor and too little electrode force is applied, liquid metal would be expelled from the molten zone and, therefore, cause expulsion. Excess metal expulsion usually results in an inconsistent and weaker weld, and it is detrimental to the weld’s engineering performance.

The heat generation pattern and nugget formation process beyond the first cycle are very much similar with those of the resistance spot welding process (Ref. 13). At the end of 1.5 cycles, the molten region has spread very rapidly toward the weld center and the molten zone is connected at the center of the weld. From this point on, the molten zone becomes ellipsoidal in shape and grows progressively in size as the welding process continues.

The final weld shape and size shown in Fig. 6 have a diameter of around 3 mm and a weld penetration of 1.2 mm. The predicted weld diameter is very close to the experimental result presented in Ref. 2 for 0.030-in. low-carbon steel. The predicted weld penetration is larger (1.2 mm vs. 0.8 mm) than the experimental result. This may be due to the slight difference in material gauges, projection design and projection wall thickness. Different machine characteristics could also contribute to the variations in different experimental results.

The comparison of the above analysis prediction with limited experimental data reported in the open literature regarding projection collapse and nugget formation process proves to be satisfactory, in general. It should be mentioned that the updating frequency in this incrementally coupled analysis is critical in achieving accurate results. In this study, the updating frequency of 1⁄16 cycle was chosen after some trial runs using larger updating frequencies failed. The necessity for using such a small updating frequency is due to the highly nonlinear coupled nature of the deformation process associated with the projection collapse process. Trial runs using an updating frequency of 1⁄32 cycle yield a very similar heating pattern and projection collapse pattern for the first cycle. Therefore, it is concluded that convergent results with respect to updating frequency can be achieved by updating every 1⁄16 cycle.

It is found that if the updating frequency is too large, the gradual increase of the contact area on the faying interface is not captured in sufficient resolution in time in the thermal-mechanical analyses. This, in turn, leads to a smaller contact area for current passage in each of the subsequent electrical-thermal analyses. A smaller contact area increases current density and would result in faster heat generation. If the predicted heat generation is too fast and the contact area is too small, the location on the faying interface outside the contact area may be melted. When this happens, the thermal-mechanical analysis would diverge because of the numerical problem encountered in trying to find an equilibrium solution with liquid metal of very low yield strength being generated outside the containment of the contact pressure. Physically, this indicates the onset of expulsion. However, in this case, it is the wrongly predicted onset of periphery melting caused by overpredicting the heat generation.

It should be noted the model does not predict full-bloom weld expulsion. Rather, it predicts the onset of expulsion in the sense of melt formation at the contact periphery and diverges afterward due to numerical difficulties. For example, Fig. 7 shows the predicted nugget shape at the end of the first cycle using an updating frequency of ¼ cycle for the same welding case presented in Fig. 6. The comparison of Fig. 7 with Fig. 6 clearly shows heat generation is overpredicted. At this moment in time, the projection has not totally collapsed, the thermal-mechanical analysis diverges and the whole analysis terminates.

Effect of Welding Current

Being a resistance welding process governed by the Joule heating principle, welding current is a very important factor in projection weld formation. It is intuitive that the weld current must be of sufficient magnitude to cause fusion before projection collapse and to form the final nugget of desired size for its engineering purpose. On the other hand, if the selected welding current is too large, the tendency for metal expulsion of a specific projection size is also increased (Ref. 2). As an example, a welding current of 8 kA is used to weld 0.8-mm SAE1010 steel sheets using the projection design shown in Fig. 1. The rest of the welding parameters remain the same as in Fig. 3. The projection and weld shape at the end of the first half cycle is shown in Fig. 8. It is shown that with this excessive current level, even with upslope control, the projection collapse cannot catch up with the speed of the heat generation. As a result, onset of expulsion is predicted.

Effect of Electrode Force

The effect of electrode force on projection collapse and nugget formation was investigated by considering two additional electrode force levels: one being 180 lb, the other being 280 lb. The rest of the welding parameters were the same as in Fig. 3. Figure 9 shows the projection collapse and heat generation for these two cases as comparisons to the nominal case shown in Fig. 6. It shows electrode force is a very influential factor in projection welding. If the electrode force is too small, it does not provide enough interface contact diameter and pressure to contain the molten metal and expulsion would occur as a result. Moreover, the projection does not collapse totally at the end of the first cycle and sheet separation is still visible. On the other hand, when too large an electrode force is applied, excessive cold set down occurs and causes premature mechanical collapse of the projection. The contact area is always bigger than that of the nominal case. Larger contact area reduces current density and, thus, delays the nugget formation process. Therefore, the art of the projection welding process lies in creating a dynamic balance between the rapid heat generation and the contact area change that will ensure nugget formation in a short period and, in the meantime, providing sufficient contact area and pressure to contain the molten metal to prevent expulsion.

Figure 10 shows a comparison of the nugget formation process for the three cases considered. The conclusion is quite similar to the conclusions reached in resistance spot welding in that the higher the electrode force, the slower the nugget growth and the smaller the final nugget. It is interesting to note, for the case with the highest electrode force, the molten zone outer radius stays at a constant level (*i.e.*, projection radius) from the first cycle to the second cycle. During this time period, the initial small ring-shaped nugget formed at the end of the first cycle grows toward the center of the weld. As a result, the center of the projection is melted at the end of the second cycle and an ellipsoidal-shaped molten zone is formed. From that point on, the nugget resumes growing outward with its final diameter being around 2.8 mm. The case with the lowest electrode force, however, diverges after onset of expulsion is detected at the end of the first cycle.

Effect of Material Properties

The steel sheet's grade and yield strength levels are also critical in projection design and welding parameter selection. For comparison purposes, the same projection design and welding parameters used earlier for SAE1010 steel are next applied to an interstitial-free (IF) steel with a room-temperature yield strength at 150 MPa and a high-strength low-alloy (HSLA) steel with a room-temperature yield strength at 440 MPa. Since yield strength and ultimate tensile strength tend to converge to similar values for most steel grades above 800°C, high-temperature mechanical properties for IF and HSLA steels are obtained by interpolation from their room-temperature values to their 800°C values following similar trends as for SAE1010. Beyond 800°C, the mechanical properties used for IF and HSLA steels are the same as those for SAE1010.

Figure 11 shows the comparison of faying interface contact radius for the three cases. For the IF steel considered, because its yield strength is too low, the cold collapse of the projection is very severe (more than 70% of the projection height) and the contact radius on the faying interface is also considerably larger than that of the nominal case of SAE1010. The welding process for this steel is very similar to the spot welding process due to the premature projection collapse, and there is no melting generated at the end of the third cycle using the welding current of 5 kA. For the projection welding of HSLA steel, on the other hand, the faying interface contact radius is significantly lower than that of the nominal case. Such a small contact radius restricts the current passage to a small area, and excessive heating and onset of expulsion occurs as early as the first half cycle — Fig. 12. Compared with the results shown in Fig. 6 for the nominal case, the projection collapse for HSLA is far behind the heat generation. There is also a difference in the heat generation pattern: no formation of the initial ring-shaped molten zone and a nugget is formed from the center of the projection.

Conclusions

In this paper, an incrementally coupled finite element analysis procedure is presented to simulate the coupled electrical-thermal-mechanical phenomena associated with the projection welding process. Projection collapse and the nugget formation process are predicted. Compared with simulations of the resistance spot welding process, projection welding involves large plastic deformation of the work sheet in the projection area, and, therefore, the analysis has to be truly "coupled" in the sense that the deformed shape of the work sheet and projection area have to be updated as well as the contact information. Effects of different welding parameters, such as welding current, electrode force and sheet material combination, have been investigated. It was found the interfacial contact behavior in the form of contact area change due to projection collapse plays a critical role in the nugget formation process in projection welding. If the electrode force is too low or an excessive welding current is used, melting occurs faster than the projection collapse and expulsion would occur as a result. On the other hand, if the applied electrode force is too high, premature collapse of the projection would cause the contact area to be too large and, therefore, reduce the current density on the faying interface and delay nugget formation. In other words, there needs to be a dynamic balance of the projection collapse and heat generation.

Commentary

It should be mentioned that, because of the large deformation involved in the analyses, it is more difficult to get converged solutions for projection welding than for spot welding, and mesh design is also critical in achieving accurate solutions. In many cases, the analysis would terminate when numerical difficulties, such as the onset of expulsion, are encountered in the simulation process.

In experimental or production environments, the welding process may continue even if some slight expulsion exists. However, the existence of expulsion would lead to inconsistency in weld quality and weld size. To reduce the occurrence of expulsion, many welding engineers choose to use a higher electrode force than the ones suggested in the handbooks (*i.e.*, Ref. 1). This practice does widen the current range for a specific projection design. However, if too high an electrode force is used, severe premature projection collapse occurs and a relatively high welding current is needed to generate an acceptable nugget size. This partially defeats the purpose of using projection welding in which relatively small electrode force and welding current can produce desirable-sized nuggets. To this end, the analysis procedure can be used as a predictive tool to optimize the welding parameters for a specific projection design to ensure nugget size and weld quality. Another application area of this tool is in the design of projection geometry for different steel grades. Results pertinent to this aspect will be presented separately.

It should also be noted the analysis procedure presented in this study is for projection welding with perfectly aligned electrodes. If the alignment is not perfect, the assumption of axisymmetry is no longer valid and a more realistic three-dimensional finite element model will need to be used.

Variations of process parameters during welding, such as electrode movements, contact area change and dynamic resistance, can also be monitored during the welding process simulation. The examples shown in this paper assume the welding machine has a perfect follow-up capability. Different machine characteristics can be incorporated in this model by specifying the electrode force profile during the entire welding process for a specific machine — or, more generically, by constructing a global dynamic model that consists of the local nugget growth model as well as the mechanical characteristics of the welding machine such as arm stiffness, weld head mass, air cylinder pressure and friction coefficient of the system.

References

1. Gould, J. E. Projection welding, *ASM Handbook*.

2. Harris, J. F., and Riley, J. J. 1961. Projection welding low carbon steel using embossed projects. *Welding Journal* 40(4): 363–376.

3. Hess, W. F., and Childs, W. J. 1947. A study of projection welding. *Welding Journal* 27(12): 712-s to 723-s.

4. Hess, W. F., Childs, W. J., and Underhill, R. F., Jr. 1949. Further studies in projection welding. *Welding Journal* 28(1): 15-s to 23-s.

5. Nippes, E. F., Gerken, J. M., and Maciora, J. G. 1950. The projection welding of 0.010- and 0.020-in. steel sheet. *Welding Journal* 29(9): 441-s to 449-s.

6. Nippes, E. F., and Gerken, J. M. 1952. Projection welding of steel in heavy gages and in dissimilar thicknesses. *Welding Journal* 31(3): 113-s to 125-s.

7. Adams, J. V., Matthews, G. N., and Begeman, M. L. 1965. Effect of projection geometry upon weld quality and strength. *Welding Journal* 44(10): 466-s to 470-s.

8. Cunningham, A., and Begeman, M. L. 1965. A fundamental study of projection welding using high speed photography. *Welding Journal* 44(8): 381-s to 384-s.

9. Cunningham, A., and Begeman, M. L. 1966. Effect of projection height upon weld quality and strength. *Welding Journal* 45(1): 26-s to 30-s.

10. Cunningham, A., Jr., Begeman, M. L., and Short, B. E. 1966. An analysis of the "nugget" formation in projection welding. *Welding Journal* 45(7): 305-s to 313-s.

11. Gould, J. E., Workman, D., and Raynes, C. 1998. An examination of projection welding coated sheet steels. *Proc. 8th Sheet Metal Welding Conf.*, Troy, Mich.

12. Nied, H. A. 1984. The finite element modeling of the resistance spot welding process. *Welding Journal* 63(4): 123-s to 132-s.

13. Tsai, C. L., Jammal, O. A., Papritan, C., and Dickinson, D. W. 1992. Modeling of resistance spot weld nugget growth. *Welding Journal* 71(2): 47-s to 54-s.

14. Sheppard, S. D. 1990. Thermal and mechanical simulations of resistance spot welding. *WRC Bulletin* 356, pp. 34–41.

15. Murakawa, H., Kimura, F., and Ueda, Y. 1997. Weldability analysis of spot welding on aluminum using FEM. *Mathematical Modeling of Weld Phenomena,* edited by H. Cerjak, pp. 944–966. The Institute of Materials.

16. Dong, P., Li, M. V., and Kimchi, M. 1997. Analysis of electrode wear mechanisms: face extrusion and pitting effects. To appear in *Science and Technology of Welding and Joining*.

17. Browne, D. J., Chandler, H. W., Evans, J. T., and Wen, J. 1995. Computer simulation of resistance spot welding in aluminum: Part I. *Welding Journal* 74(10): 339-s to 344-s.

18. Browne, D. J., Chandler, H. W., Evans, J. T., James, P. S., Wen, J., and Newton, C. J. 1995. Computer simulation of resistance spot welding in aluminum: Part II. *Welding Journal* 74(12): 417-s to 422-s.

19. Li, M. V., Dong, P., and Kimchi, M. 1997. Modeling of contact resistance during resistance spot welding. *Proc. 7th Int. Conf. on Computer Tech. in Welding.* Ed. T. Siewert, pp. 423–435. NIST Special Publication 923, United States Department of Commerce.

20. Sun, X., and Dong, P. Analysis of aluminum resistance spot welding processes using coupled finite element procedures. *Welding Journal* 79(8): 215-s to 221-s.

21. *ABAQUS/Standard and ABAQUS/Explicit User's Manuals*, Version 5.8. Hibbitt, Karlsson & Sorensen, Inc.

22. Properties and selections: irons and steels. 1978. *Metals Handbook,* 9th edition, Vol. 1 and 2.

23. Barber, J. R. 1992. *Elasticity.* Kluwer Academic Publishers, the Netherlands.

24. *High-Temperature Property Data: Ferrous Alloys.* 1988. ASM International, Materials Park, Ohio.

25. *Physical Constants of Some Commercial Steels at Elevated Temperatures.* 1953. Edited by The British Iron and Steel Research Association. Butterworths Scientific Publications, London, U.K.